Smith Erik (Orcid ID: 0000-0002-8133-0348)
Lee Cameron (Orcid ID: 0000-0002-5380-6601)

Assessing trends in atmospheric circulation patterns across North America

Erik T. Smith*

Omon Obarein

Scott C. Sheridan

Cameron C. Lee

Kent State University; Department of Geography

*Corresponding Author Information: esmit149@kent.edu; ORCID: 0000-0002-8133-0348

Abstract

Circulation patterns (CPs) are discrete categorizations of spatial fields of atmospheric conditions, often used to examine the interaction between the overlying atmosphere and surface weather. Examining changes in the frequency of these atmospheric CPs may therefore help us better understand the relationship between a changing climate and the occurrence of extreme weather events. In this study, we use self-organized maps (SOMs) to classify CPs from 500mb geopotential heights (500z) and mean sea-level pressure (MSLP) for five regions across North America, using two different reanalysis datasets. Trends in CPs (from 1979-2018) from both the North American Regional Reanalysis (NARR) and the recently released ERA5 datasets are compared using a new method in which the CPs from the ERA5 dataset are based on the principal components of the NARR data. This results in a more direct comparison between the CPs of each dataset. z500 CP trends were generally larger than the MSLP CP trends and the NARR CP trends were generally larger than the ERA5 CP trends. Furthermore, the most extreme summer-dominant CPs were found to have increased significantly over the 40-year study period in all five regions for both the NARR and ERA5 CPs.

Key Words: synoptic climatology, atmospheric circulation patterns, ERA5, NARR, North America, self-organized maps

This is the author manuscript accepted for publication and has undergone full peer review but has not been through the copyediting, typesetting, pagination and proofreading process, which may lead to differences between this version and the Version of Record. Please cite this article as doi: 10.1002/joc.6983

Introduction

Fluctuations in synoptic-scale atmospheric circulation patterns (CPs) can explain much of the interannual variability in surface weather across the Northern Hemisphere (Feldstein & Franzke, 2017). While internal variability can explain seasonal fluctuations in the spatial and temporal distribution of CPs, long-term changes in CPs can be impacted by external forcing such as anthropogenic warming (Frankcombe et al. 2015; Hua, Dai, & Qin, 2018; Mitchel et al., 2016). Fluctuations in CPs have been associated with an increased frequency of extreme weather events (Horton et al. 2015; Gao et al., 2019), therefore, quantifying the long-term changes are important for identifying regions with an increased susceptibility to extreme events. As observed changes in CPs are dependent on the dataset used for the analysis, several studies have compared trends in CPs derived from multiple datasets (Barnes et al., 2014; Horton et al. 2015; & Screen; Simmonds 2013). However, due to discrepancies between datasets, studies that compare CPs from multiple datasets often cluster the CPs individually then use a statistical technique, such as root mean squared error (RMSE), to identify the CPs most similar to one another (Horton et al. 2015). Even then, the observed trend between similar CPs cannot be directly compared; rather, the statistical relationship between the two CPs must first be considered.

CP classification is a technique used to discretize atmospheric circulation by reducing continuous data into well-defined categories, or CPs, through methods such as self-organized maps (SOMs), k-means clustering, or empirical orthogonal functions (EOFs). By reducing the dimensionality of the data, the relationship between the atmospheric and surface weather may be more readily understood. Changes in atmospheric CPs have been linked with changes in atmospheric and oceanic phenomena such as the North Atlantic Oscillation (NAO; Saaroni et al., 2019; Putnikovic et al., 2018; Cherenkova & Semenov, 2017) the Arctic Oscillation (AO) via Arctic amplification (Francis, Skific, & Vavrus, 2018), the El Niño Southern Oscillation (ENSO; Grainger et al., 2017), and the Atlantic Multidecadal Oscillation (AMO; Cherenkova & Semenov, 2017). Many of the studies that examine changes in the frequency of CPs are typically interested in better understanding how these changes are associated with extreme surface weather events. Extreme events have been linked to the occurrence of CPs by

establishing consistencies between the spatiotemporal distribution of anomalous CPs and surface weather anomalies (Gao et al., 2019). CPs of mean sea-level pressure (MSLP) and 500mb geopotential heights (500z) have been linked to extreme heat, extreme cold, droughts, and extreme precipitation events (Nicholson et al., 2018; Farukh & Yamada, 2018; Cassano et al., 2016). Positive z500 and MSLP anomalies were found to increase the likelihood of extreme heat across Europe and Brazil (Geirinhas et al., 2018; Tomczyk et al., 2017; Tomczyk, 2017). These extreme heat events may exacerbate drought conditions, which reinforce the extreme heat by increasing the positive z500 anomalies (Ionita et al., 2017; Trigo et al., 2005) and MSLP anomalies (Tomczyk et al., 2019). Conversely, negative z500 anomalies were associated with negative MSLP anomalies which favour extreme precipitation events (Liu et al., 2016; Lolis & Turkes, 2016). Horton et al. (2015) used SOMs to identify trends in CPs across the Northern Hemispheric mid-latitudes and found anticyclonic CPs in Eurasia and North America had increased. Maheras et al. (2018) used a synoptic pattern classification to classify CPs over Europe and found that cyclonic CPs, associated with heavy precipitation events, showed a positive trend, while the anticyclonic CPs, associated with fewer heavy precipitation events, showed a negative trend. The results of this study are corroborated by other studies for Europe (Kysely & Huth, 2006; Bertoszek, 2017).

Reanalysis datasets have greatly facilitated the analysis of atmospheric CPs due to their large temporal extent and spatially continuous nature. Two such datasets, the North American Regional Reanalysis (NARR) and ECMWF ERA5 reanalysis datasets, were developed for different domains by using different models and parameterizations, making data discrepancies inevitable. The ERA5, which is the most recent ECMWF global reanalysis product, has been shown to be a sizeable improvement over the ERA-Interim reanalysis product, namely due to an increase in the spatial and temporal resolution (Hoffmann et al., 2019; Urraca et al., 2018). The NARR, however, is a high-resolution subset of the NCEP-NCAR Global reanalysis optimized to better resolve regional atmospheric variables over North America (Mesinger at al., 2006).

Since no single reanalysis dataset can perfectly resolve atmospheric or oceanic processes, using multiple reanalysis datasets to examine spatial and temporal changes in CPs can help

reveal uncertainties in these changes. As such, this study uses self-organized maps (SOMs) to categorize CPs from MSLP and z500 data for six regions across North America from both the NARR and ERA5 reanalysis datasets. To limit the ambiguity of comparing CPs from different datasets, this study develops a more direct method to compare trends in CP frequency between the NARR and ERA5 for each region.

Data and Methods

Daily mean values of mean sea-level pressure (MSLP) and 500 mb geopotential heights (z500) were derived from the North American Regional Reanalysis (NARR; Mesinger et al., 2006) dataset from 1979 through 2018 (Table 1). Hourly MSLP and geopotential were derived from the European Centre for Medium-Range Weather Forecasting (ECMWF) ERA5 Reanalysis dataset (Hersbach, 2018; Copernicus Climate Change Service, 2017) and converted to mean daily values. The ERA5 geopotential data were then converted to geopotential *heights* by dividing by the acceleration of gravity. Both the ERA5 and NARR data were downloaded for the entire NARR domain [12.2N; 133.5W, 54.5N; 152.9W, 57.3N; 49.4W ,14.3N; 65.1W] at a spatial resolution of 0.3^{o} [32km] (NARR) and 0.25^{o} [31km] (ERA5). Because the focus of this research was on the large-scale trends across North America, the data was upscaled to reduce computational requirements. The NARR data was upscaled to a spatial resolution of approximately 192 km and the ERA5 data interpolated using a Delaunay triangulation of the gridded data points to match the grid of the upscaled NARR. Delaunay triangulation, which has been used in previous climate studies, is a more efficient interpolation method that is generally less affected by artefacts within the data than other methods such as inverse distance weighting (Amidror, 2002; Ringler, Ju, & Gunzburger, 2008).

North America was separated into five overlapping regions: eastern United States (East), south-eastern United States and Gulf of Mexico (Gulf), western United States (West), western Canada and Alaska (North), and eastern Canada (Canada) (Figure 1). Circulation patterns (CPs) were categorized through the creation of SOMs based on each of the MSLP and z500 data from the NARR and ERA5 datasets for each of the five regions. SOMs are particularly useful when classifying a large number of patterns from high dimensional data and visualizing the

resultant patterns as a continuum, whereby similar patterns are located nearest to each other and less similar patterns further apart in a two-dimensional SOM space (Sheridan and Lee, 2011; Hewitson & Crane, 2002). The number of clusters along with the horizontal and vertical dimensions of the SOM were determined through five internal clustering validation metrics: the Calinski-Harabasz criterion, the Davies-Bouldin criterion, the Silhouette criterion, the Variability Skill Score (Lee, 2014) and the Distributed Variability Skill Score (Lee, 2017), evaluated across all 49 possible options from a 3x3 to a 9x9 SOM size.

Before using a SOM to classify CPs, an s-mode principal components analysis (PCA) was run on the z-scores of the data to reduce computational time (via dimension reduction) and mitigate spatial collinearity prior to clustering. PCA is a multivariate statistical technique widely used in the atmospheric sciences to reduce a large number of variables into much fewer, more manageable variables (Bednorz et al., 2019). Principal components (PCs) with eigenvalues greater than 1 retained to be used in the classification (Sheridan & Lee, 2011). Because the SOM is an unsupervised neural network algorithm, it must be trained through an iterative process whereby a predefined number of nodes (determined via the cluster validation mentioned above) that form the lattice of the SOM, migrate via a user-defined learning rate parameter from a randomly initialized starting point towards regions of more dense data points (Hewitson & Crane, 2002). The result is a time series of nodes, or clusters, where each day in the time period is classified by a single cluster number. The SOM maps, comprised of individual CPs, are produced by compositing the daily gridded data from all days classified into the cluster/node.

Comparing NARR and ERA5 circulation pattern trends

Comparing trends in CPs created from multiple datasets is difficult as there is no agreed-upon way of clustering the data such that the resultant CPs from each dataset can be objectively matched. However, a nearly identical SOM can be created by using a PCA and the neural network data derived from the same variable of another dataset. While discrepancies between the ERA5 and NARR datasets are inevitable, particularly near the boundary of the NARR domain (as shown below), nearly all the variance within each variable can be explained

by the same few dimensions, or principal components. Hence, this method uses the dimensions of the data that explain approximately 99% of the variance within the NARR dataset as the input for the ERA5 SOM. This results in nearly identical CPs, represented by separate SOMs, and a separate timeseries of CPs for the NARR and ERA5, allowing the spatial and temporal similarity to be measured. This method is outlined in the following steps:

1. A PCA of the z-scores of the NARR dataset was used to reduce the dimensionality of the data and then input into the SOM algorithm to classify the retained principal components (PCs) into a daily timeseries of CPs.
2. The ERA5 was interpolated to match the grid of the NARR dataset and the z-scores calculated for the re-gridded ERA5 dataset.
3. The PC loadings matrix calculated from the NARR PCA, were multiplied by the ERA5 z-scores to create 'virtual PCs' for the ERA5 data which mimic those of the NARR. The number of retained PCs for the ERA5 variables were determined by the retained PCs of the same NARR variable.
4. The retained ERA5 PCs were then used as the input into the saved SOM (the artificial neural network) created from the NARR data for the same variable and region.

Spatial similarity between the NARR and ERA5 SOMs was determined by calculating the correlation between the mean values at each grid point for each CP between the two datasets. Because correlations cannot quantify systematic differences between the datasets, a mean absolute error (MAE) of the standardized NARR and ERA5 CP means was also calculated for each region. The CP means were standardized by turning both the NARR and ERA5 CP means into z-scores for each grid point. Standardization was used because the MAE for each region is dependent on scale, climate, and the latitudinal and longitudinal extent of the region's domain. Regions with high variability are more likely to have a higher MAE than regions with comparatively lower variability. The North region, comprised of Alaska and the Yukon, experiences a much larger range in z500 than the more tropical Gulf region. Similarly, the Gulf region has much lower MSLP variability than the North region, which captures modulations in the Aleutian Low. Thus, comparisons of non-standardized MAEs between regions would be difficult. The mean CP MAE for each SOM and region is shown in Table 2.

Temporal similarity was determined by calculating the total and yearly percentage in which the NARR and ERA5 CPs occurred on the same day over the 40-year period. Because the SOMs were nearly identical, only the NARR SOMs are shown in the discussion for each region, with the exception of the East region for initial comparisons. To simplify the discussion, each CP is denoted by the dataset, NARR (N) and ERA5 (E), followed by the pattern number. CP 1 for the ERA5 SOM would be denoted as E1 and N1 for the NARR SOM. These naming conventions are used for each region in the discussion.

The Gulf region exhibited the largest differences between the ERA5 and NARR, therefore, a sixth region (New Gulf) was added to determine the degree to which the large longitudinal extent, which encompasses the Bermuda High and the Sierra Madre Mountains, impacted the clustering solutions in the Gulf region. Because the New Gulf region had a much smaller longitudinal extent than the original Gulf domain, only 10 CPs were used in the New Gulf SOM compared with the original 20 CPs. The choice to reduce the number of CPs was supported by the above-mentioned cluster validation metrics, which were computed for the New Gulf region.

Annual trends in z500 and MSLP CPs were calculated for each region for the 40-year period of 1979 – 2018. A Theil-Sen slope estimation, computed from 1000 bootstrapped resamples of the annual CP frequency, was used to estimate the change/slope in the annual frequency of each CP. Statistical significance of the slope was determined if the 95% confidence intervals produced from the bootstrapped resamples did not contain zero.

Results and Discussion

NARR vs ERA5

For all regions except the Gulf, the NARR and ERA5 CPs are very similar. MSLP, being a near-surface variable, has greater variability in its spatial patterns than z500 and is likely the reason that the NARR and ERA5 z500 CPs are more spatially similar than the MSLP CPs. The z500 and MSLP SOMs for the East, West, North, and Canada regions were most similar, with correlations between the individual CP gridpoints exceeding 0.99 and low mean absolute errors (MAE; Table 2). This suggests that the NARR and ERA5 CPs in these four regions are both strongly related and spatially similar. However, the Gulf region had a much higher MAE

and lower individual CP gridpoint correlations than the other regions. These discrepancies may be attributed to the Gulf region being near the edge of the NARR domain (Warner, Peterson, & Treadon, 1997; Zick & Matyas, 2015) or to how each reanalysis dataset resolves certain processes and are likely exacerbated by the data sparsity of the Gulf of Mexico, relative to the data-richness over land, and complexities introduced by the Sierra Madre Mountains and the Bermuda High.

The temporal similarity, much like the spatial similarity, was highest for the East, West, North, and Canada regions, with the z500 and MSLP SOM CPs matching between 86% and 92% of all days in the record, and lowest for the Gulf region with the SOM CPs matching 67% (MSLP) and 69% (500z) of all days (Table 2). Yearly fluctuations in the mean SOM CP match percentage are shown in Figure 2. While there is no trend in the yearly match percentages for any region, there are systematic fluctuations evident in many regions. The five-year period from 2002 – 2007 experienced a 10% to 20% drop in z500 CP match percentages across each region, followed by a systematic increase from 2007 – 2012. This suggests that discrepancies between reananalysis datasets may be affected by low-frequency atmospheric or oceanic variability. However, it may also be due to changes in the way data is integrated into the reanalysis datasets, such as an increase in observational measurements (Dee et al., 2016). Both temporal and spatial similarity tended to be higher for the more extreme CPs at the edge of the SOM, while the less extreme CPs, generally near the center of the SOM, had lower CP match percentages, higher MAE, and lower correlations.

The New Gulf region, which was added to better understand the discrepancies between the NARR and ERA5 z500 and MSLP SOMs in the original Gulf region, showed improvement in both the spatial and temporal similarity (Table 2; Figure 2). The MSLP SOM CP match percentage improved to 85%, while the z500 SOM improved to 78%. The improvement in the temporal similarity can likely be attributed to the fewer patterns in the New Gulf SOM. With fewer CPs, the differences between each CP are larger, thus the likelihood that a particular day is categorized differently between the NARR and ERA5 is lowered. However, the MAE of the New Gulf z500 and MSLP SOMs decreased by approximately half the original MAE. This improvement in spatial similarity for the New Gulf SOMs, along with the improved temporal

similarity, suggests the longitudinal extent of the original Gulf region may have exacerbated the descrepencies between the NARR and ERA5 CPs. For this reason, the domain of the dataset should be strongly considered when clustering atmospheric data as large spatial variability in the domain can impact the CPs.

Circulation Pattern (CP) Trends

Summer-dominant z500 CPs have significantly increased in frequency in every region since 1979. Winter-dominant z500 CP trends, though generally smaller in magnitude and less-often signficant than the summer-dominant CP trends, have decreased in frequency in most regions. While the magnitude of the z500 CP changes are not always consistent between the NARR and ERA5 SOMs, the significance is generally consistent. Both the NARR and ERA5 show winter-dominant high MSLP CPs have increased significantly in the Gulf of Alaska, interior Alaska, and the Yukon since 1979. This trend may partially explain the recent warming across Alaska (Walsh & Brettschneider, 2019). Although the NARR and ERA5 both show this MSLP trend, other significant MSLP trends are not consistent between the NARR and ERA5. The trends in z500 CPs are generally larger and more often significant than the MSLP CP trends, while also being more consistent between the NARR and ERA5. Because of this, the remaining discussion focuses on the regional z500 trends.

East Region

The CPs from the z500 SOM for the East region are very similar between the NARR (Figure 3) and ERA5. The SOM is oriented such that the most extreme summer-dominant pattern (highest heights) is located in the upper left corner and the most extreme winter-dominant pattern (lowest heights) is located in the bottom right corner. CPs 8 and 10 have decreased significantly for both the NARR and ERA5. CP 8 is a transitional CP, occurring autumn through the spring, while CP 10 is primarily a late winter and early spring CP. The warmest z500 CP experienced the largest 40-year change with an increase of 34 (N21) and 15 (E21) occurrences. The large discrepancy between N21 and E21 is due to CPs being different enough to be categorized as adjacent CPs. N16 occurred more frequently than E16 early in the study period but at a similar frequency toward the end of the study period, thus the decrease in the number of occurrences of N16 is larger than E16 while the increase in the frequency of N21 is greater than the increase in E21 occurrences. Nonetheless, both the ERA5 and NARR trends

suggest warm-extreme CPs during the summer are becoming more likely across the eastern United States.

Canada Region

As with the East Region, summer-dominant CPs in the Canada region (Figure 4) exhibited the largest positive trends with an increase of 23 (14) and 11 (14) annual occurrences for N5 (E5) and N10 (E10) over the full period of record. Unlike the summer-dominant CPs, winter-dominant CPs have exhibited a negative trend over the past 40 years, though generally non-significant. N11 and E17, which are late-autumn to early spring CPs, are the only winter-dominant CPs with a significant positive trend. The increasing prevalence of the two warmest CPs suggests the likelihood of extreme heat in Canada has increased over the last 40 years (e.g. Lee and Sheridan, 2018). Furthermore, the large increase in CPs 5 and 10 comes at the expense of less extreme CPs, which have decreased non-significantly over the past 40 years.

Gulf Region

Variability in the Gulf region is an expression of modulations in the Inter-Tropical Convergence Zone (ITCZ), the subtropical-high near Bermuda, the Pacific and Atlantic Oceans, and the Sierra Madre Mountains (Figures 5 and 6). The trends for the New Gulf region (Figure 6) are much larger than the trends of the original Gulf region (Figure 5) because there are fewer CPs. However, both the NARR and ERA5 Gulf and New Gulf z500 SOMs show a large positive trend in summer and autumn-dominant CPs, with the warmest CP (Gulf: CP 25, New Gulf: CP 6) exhibiting the largest increase of any CP for any region. Conversely, winter and spring-dominant CPs have decreased significantly in both the NARR and ERA5 Gulf and New Gulf SOMs, suggesting a systematic shift from cooler to warmer CPs in and around the Gulf of Mexico. Though the differences between the NARR and ERA5 are the largest in the Gulf region, the CP trends are relatively consistent. Moreover, the CP trends in the original Gulf SOM are evident in the New Gulf SOM, further supporting the systematic shift toward warmer CPs in this region.

North Region

The North region, centered on Alaska and the Yukon, is a region that has experienced large changes in atmospheric circulation in recent decades (Figure 7; McLeod, Ballinger, & Mote, 2018). In addition to the downstream implications of variability in this region, changes in CPs in this region are thought to be contributing to large sea-ice loss in the Bering, Beaufort, and Chukchi Seas (Ballinger et al., 2019; Ballinger & Rogers, 2013; Ballinger & Sheridan, 2014; Walsh et al., 2017). While both the NARR and ERA5 show a decrease in winter-dominant CPs, only the change in CP 23 is significant. CP 23, which is a less extreme troughing CP and occurs most frequently from the autumn through the spring, has increased by 8 days compared to the beginning of the study period, while surrounding SOM CPs have decreased. As seen in the other regions, the most extreme summer-dominant CP (CP 19) has exhibited a large increase in the number of occurrences per year, with N19 (E19) occurring 18 (11) more days annually at the end of the period compared to the beginning. Also noted by Walsh & Brettschneider (2019), the more extreme winter-dominant CPs have declined while less extreme winter-dominant CPs across the Gulf of Alaska have become more prevalent and may be contributing to the record-warm temperatures and sea-ice loss across the region. Furthermore, an increase in ridging CPs near the Gulf of Alaska with a decrease in extreme winter-dominant CPs in this region may contribute to an increased frequency of downstream troughing and prolonged periods of extreme cold in central and eastern North America. (Vavrus et al., 2006).

West Region

Similar to the other regions, the warmest CP in the Western region z500 SOM (Figure 8) exhibited the largest increase of 18 days (N1) and 11 days (E1) since the beginning of the study period. Also evident in the North region, autumn and spring dominant CPs have increased in frequency (CP 6) while winter dominant CPs have decreased in frequency (CP 8). As noted by Wise (2016), ridging across the western United States leads to warmer temperatures and less precipitation, and this compounding of warmer temperatures and little to no precipitation increases the likelihood of severe drought in this region. Therefore, the observed increase in summer-dominant CPs, particularly from late-spring through autumn, may result in an increased susceptibility to wildfires in the western United States (Holden et al., 2018).

Conclusions

Atmospheric CPs have been linked to extreme weather events, therefore understanding long-term trends in CPs may improve the prediction and understanding of trends in extreme weather events. These trends are often calculated using different reanalysis products, each with small nuances and systematic biases in resolving the atmosphere. The discrepencies between the CPs derived from the NARR and ERA5 in this study are a reminder that no single reanalysis dataset is perfect, and thus utilizing multiple datasets can provide a more robust perspective on changes in CPs. However, it is these discrepencies that make comparing CPs between different renalysis datasets difficult. The method outlined in this study creates near-identical CPs for both z500 and MSLP variables from both datasets in all domains of the study. Even the CPs for Gulf region, which were the most different between the NARR and ERA5, resulted in very similar CPs from a quantitivate sense, and nearly identical CPs visually. Still, the differences between CPs in the Gulf region highlight the need to consider complex processes, such as the surface-atmosphere and ocean-atmosphere interaction, when categorizing CPs, along with potential discrepencies related to the datasets domain boundaries.

While NARR CP trends are generally larger than the respective ERA5 CP trends, both reanalysis datasets agree that warm extremes have increased in frequency significantly since 1979 while cold extremes have decreased in frequency in all five regions. An increase in warm CPs may be linked with decreasing sea-ice, prolonged periods of anomolous warmth, and an increase in drought and wildfires. The increase in warm extreme z500 CPs with a decrease in cold extreme z500 CPs supports the notion that climate change can manifest in the systematic shift in CPs (Horton et al., 2015; Mitchell et al., 2016; Tomczyk, 2017; Walsh & Brettschneider, 2019). However, the increase in warm-extreme z500 CPs may also be a result of thermal expansion as the climate warms (Cattiaux et al., 2013; Swain et al., 2016), which could explain the differences in the trends of the MSLP and z500 CPs.

This study can be used to better understand how changes in CPs, particularly the extreme CPs, may be affecting human thermal comfort. Future work will use this CP comparison

method to examine changes in the frequency and duration of CPs during the autumn and spring which may be contributing to prolonged heat across regions of North America with anomalous early-season cold in other regions. Additional research will also explore the impact of low-frequency atmospheric or oceanic circulations on discrepancies in CPs derived from different reanalysis datasets.

Acknowledgments

This research was supported by federal award number NA17OAR4310159, entitled "Developing extreme event climate change indicators related to human thermal comfort" from the National Oceanic and Atmospheric Administration's Climate Program Office.

References

Amidror, I. (2002). Scattered data interpolation methods for electronic imaging systems: a survey. *Journal of Electronic Imaging*, 157-76.

Ballinger, T.J., Lee, C.C., Sheridan, S.C., Crawford, A.D., Overland, J.E. and Wang, M. (2019). Subseasonal atmospheric regimes and ocean background forcing of Pacific Arctic sea ice melt onset. *Climate Dynamics*, 52(9-10), pp.5657-5672.

Ballinger, T. J., & Rogers, J. C. (2013). Atmosphere and ocean impacts on recent western Arctic summer sea ice melt. *Geography Compass*, 7(10), 686-700.

Ballinger, T. J., & Sheridan, S. C. (2014). Associations between circulation pattern frequencies and sea ice minima in the western Arctic. *International Journal of Climatology*, 34(5), 1385-1394.

Barnes, E. A., Dunn-Sigouin, E., Masato, G., & Woollings, T. (2014). Exploring recent trends in Northern Hemisphere blocking. *Geophysical Research Letters*, 41(2), 638-644.

Bartholy, J., Pongrácz, R., & Gelybó, G. (2009). Climate signals of the North Atlantic Oscillation detected in the Carpathian basin. *Applied Ecology and Environmental Research*, *7*(3), 229-240.

Bartoszek, K. (2017). The main characteristics of atmospheric circulation over East-Central Europe from 1871 to 2010. *Meteorology and Atmospheric Physics*, *129*(2), 113-129.

Bednorz, E., & Wibig, J. (2017). Circulation patterns governing October snowfalls in southern Siberia. *Theoretical and Applied Climatology*, *128*(1-2), 129-139.

Cassano, J. J., Cassano, E. N., Seefeldt, M. W., Gutowski Jr, W. J., & Glisan, J. M. (2016). Synoptic conditions during wintertime temperature extremes in Alaska. *Journal of Geophysical Research: Atmospheres*, 121(7), 3241-3262.

Cherenkova, E. A., & Semenov, V. A. (2017). A link between winter precipitation in Europe and the Arctic Sea ice, sea surface temperature, and atmospheric circulation. *Russian Meteorology and Hydrology*, 42(4), 238-247.

Copernicus Climate Change Service (C3S) (2017): ERA5: Fifth generation of ECMWF atmospheric reanalyses of the global climate. Copernicus Climate Change Service Climate Data Store (CDS), March 23, 2019.

Dee, Dick, Fasullo, John, Shea, Dennis, Walsh, John & National Center for Atmospheric Research Staff (Eds). Last modified 12 Dec 2016. "The Climate Data Guide: Atmospheric Reanalysis: Overview & Comparison Tables." Retrieved from https://climatedataguide.ucar.edu/climate-data/atmospheric-reanalysis-overview-comparison-tables.

Farukh, M. A., & Yamada, T. J. (2018). Synoptic climatology of winter daily temperature extremes in Sapporo, northern Japan. *International Journal of Climatology*, 38(5), 2230-2238.

Francis, J. A., Skific, N., & Vavrus, S. J. (2018). North American weather regimes are becoming more persistent: Is Arctic amplification a factor?. *Geophysical Research Letters*, 45(20), 11-414.

Frankcombe, L. M., England, M. H., Mann, M. E., & Steinman, B. A. (2015). Separating internal variability from the externally forced climate response. *Journal of Climate*, 28(20), 8184-8202.

Feldstein, S. B., & Franzke, C. L. (2017). Atmospheric teleconnection patterns. *Nonlinear and Stochastic Climate Dynamics*, 54-104.

Gao, M., Yang, Y., Shi, H., & Gao, Z. (2019). SOM-based synoptic analysis of atmospheric circulation patterns and temperature anomalies in China. *Atmospheric Research*, *220*, 46-56.

Geirinhas, J. L., Trigo, R. M., Libonati, R., Coelho, C. A., & Palmeira, A. C. (2018). Climatic and synoptic characterization of heat waves in Brazil. *International Journal of Climatology*, 38(4), 1760-1776.

Grainger, S., Frederiksen, C. S., & Zheng, X. (2017). Projections of Southern Hemisphere atmospheric circulation interannual variability. *Climate Dynamics*, 48(3-4), 1187-1211.

Hersbach, H. (2018). Operational global reanalysis: progress, future directions and synergies with NWP. European Centre for Medium Range Weather Forecasts.

Hoffmann, L., Günther, G., Li, D., Stein, O., Wu, X., Griessbach, S., ... & Wright, J. S. (2019). From ERA-Interim to ERA5: the considerable impact of ECMWF's next-generation reanalysis on Lagrangian transport simulations. *Atmospheric Chemistry and Physics*, *19*(5), 3097-3124.

Holden, Z. A., Swanson, A., Luce, C. H., Jolly, W. M., Maneta, M., Oyler, J. W., ... & Affleck, D. (2018). Decreasing fire season precipitation increased recent western US forest wildfire activity. *Proceedings of the National Academy of Sciences*, 115(36), E8349-E8357.

Horton, D. E., Johnson, N. C., Singh, D., Swain, D. L., Rajaratnam, B., & Diffenbaugh, N. S. (2015). Contribution of changes in atmospheric circulation patterns to extreme temperature trends. *Nature*, 522(7557), 465.

Hewitson, B. C., & Crane, R. G. (2002). Self-organizing maps: applications to synoptic climatology. *Climate Research*, *22*(1), 13-26.

Hua, W., Dai, A., & Qin, M. (2018). Contributions of internal variability and external forcing to the recent Pacific decadal variations. *Geophysical Research Letters*, 45(14), 7084-7092.

Ionita, M., Tallaksen, L., Kingston, D., Stagge, J., Laaha, G., Van Lanen, H., ... & Haslinger, K. (2017). The European 2015 drought from a climatological perspective. *Hydrology and Earth System Sciences*, 21, 1397-1419.

Kyselý, J., & Huth, R. (2006). Changes in atmospheric circulation over Europe detected by objective and subjective methods. *Theoretical and Applied Climatology*, *85*(1-2), 19-36.

Lee, C.C. and Sheridan, S.C., 2018. Trends in weather type frequencies across North America. *NPJ Climate and Atmospheric Science*, 1(1), p.41.

Lee, C. C. (2015). The development of a gridded weather typing classification scheme. *International Journal of Climatology*, 35(5), 641-659.

Lee, C. C. (2017). Reanalysing the impacts of atmospheric teleconnections on cold-season weather using multivariate surface weather types and self-organizing maps. *International Journal of Climatology*, 37(9), 3714-3730.

Liu, W., Wang, L., Chen, D., Tu, K., Ruan, C., & Hu, Z. (2016). Large-scale circulation classification and its links to observed precipitation in the eastern and central Tibetan Plateau. *Climate Dynamics*, 46(11-12), 3481-3497.

Lolis, C. J., & Türkeş, M. (2016). Atmospheric circulation characteristics favoring extreme precipitation in Turkey. *Climate Research*, 71(2), 139-153.

Maheras, P., Tolika, K., Anagnostopoulou, C., Makra, L., Szpirosz, K., & Károssy, C. (2018). Relationship between mean and extreme precipitation and circulation types over Hungary. *International Journal of Climatology*, *38*(12), 4518-4532.

McLeod, J. T., Ballinger, T. J., & Mote, T. L. (2018). Assessing the climatic and environmental impacts of mid-tropospheric anticyclones over Alaska. *International Journal of Climatology*, 38(1), 351-364.

Mesinger, F., DiMego, G., Kalnay, E., Mitchell, K., Shafran, P. C., Ebisuzaki, W., ... & Ek, M. B. (2006). North American regional reanalysis. *Bulletin of the American Meteorological Society*, *87*(3), 343-360.

Mitchell, D., Heaviside, C., Vardoulakis, S., Huntingford, C., Masato, G., Guillod, B. P., ... & Allen, M. (2016). Attributing human mortality during extreme heat waves to anthropogenic climate change. *Environmental Research Letters*, 11(7), 074006.

Nicholson, C., Shinker, J. J., Hanway, V. M., & Zavala, S. (2018). The Influence of Atmospheric Circulation on Abnormal Snowpack Melt-Out Events and Drought in Wyoming. *JAWRA Journal of the American Water Resources Association*, 54(6), 1355-1371.

Ning, L., & Bradley, R. S. (2015). Winter climate extremes over the northeastern United States and southeastern Canada and teleconnections with large-scale modes of climate variability. *Journal of Climate*, 28(6), 2475-2493.

Putniković, S., Tošić, I., Lazić, L., & Pejanović, G. (2018). The influence of the large-scale circulation patterns on temperature in Serbia. *Atmospheric Research*, *213*, 465-475.

Ringler, T., Ju, L., & Gunzburger, M. (2008). A multiresolution method for climate system modeling: Application of spherical centroidal Voronoi tessellations. *Ocean Dynamics*, 58(5-6), 475-498.

Saaroni, H., Ziv, B., Harpaz, T., & Lempert, J. (2019). Dry events in the winter in Israel and its linkage to synoptic and large-scale circulations. *International Journal of Climatology*, 39(2), 1054-1071.

Screen, J. A., & Simmonds, I. (2013). Exploring links between Arctic amplification and

mid-latitude weather. *Geophysical Research Letters*, 40(5), 959-964.

Sheridan, S. C., & Lee, C. C. (2011). The self-organizing map in synoptic climatological research. *Progress in Physical Geography*, *35*(1), 109-119.

Tomczyk, A. M. (2017). Atmospheric circulation during heat waves in Eastern Europe. *Geografie*, 122(2), 121-146.

Tomczyk, A., Półrolniczak, M., & Bednorz, E. (2017). Circulation conditions' effect on the occurrence of heat waves in western and southwestern Europe. *Atmosphere*, *8*(2), 31.

Tomczyk, A. M., Bednorz, E., & Polrolniczak, M. (2019). The occurrence of heat waves in Europe and their circulation conditions. *Geografie*, 124(1), 1-17.

Trigo, R. M., García-Herrera, R., Díaz, J., Trigo, I. F., & Valente, M. A. (2005). How exceptional was the early August 2003 heatwave in France? *Geophysical Research Letters*, 32(10).

Urraca, R., Huld, T., Gracia-Amillo, A., Martinez-de-Pison, F. J., Kaspar, F., & Sanz-Garcia, A. (2018). Evaluation of global horizontal irradiance estimates from ERA5 and COSMO-REA6 reanalyses using ground and satellite-based data. *Solar Energy*, *164*, 339-354.

Vavrus, S., Walsh, J. E., Chapman, W. L., & Portis, D. (2006). The behavior of extreme cold air outbreaks under greenhouse warming. *International Journal of Climatology: A Journal of the Royal Meteorological Society*, 26(9), 1133-1147.

Walsh, J. E., & Brettschneider, B. (2019). Attribution of recent warming in Alaska. *Polar Science*, 21, 101-109.

Walsh, J. E., Fetterer, F., Scott Stewart, J., & Chapman, W. L. (2017). A database for depicting Arctic sea ice variations back to 1850. *Geographical Review*, 107(1), 89-107.

Warner, T. T., Peterson, R. A., & Treadon, R. E. (1997). A tutorial on lateral boundary conditions as a basic and potentially serious limitation to regional numerical weather prediction. *Bulletin of the American Meteorological Society*, 78(11), 2599-2618.

Wise, E. K. (2016). Five centuries of US West Coast drought: Occurrence, spatial distribution, and associated atmospheric circulation patterns. *Geophysical Research Letters*, 43(9), 4539-4546.

Yu, B., & Lin, H. (2019). Modification of the wintertime Pacific–North American pattern related North American climate anomalies by the Asian–Bering–North American teleconnection. *Climate Dynamics*, 53(1-2), 313-328.

Zick, S. E., & Matyas, C. J. (2015). Tropical cyclones in the North American Regional Reanalysis: An assessment of spatial biases in location, intensity, and structure. *Journal of Geophysical Research: Atmospheres*, 120(5), 1651-1669.

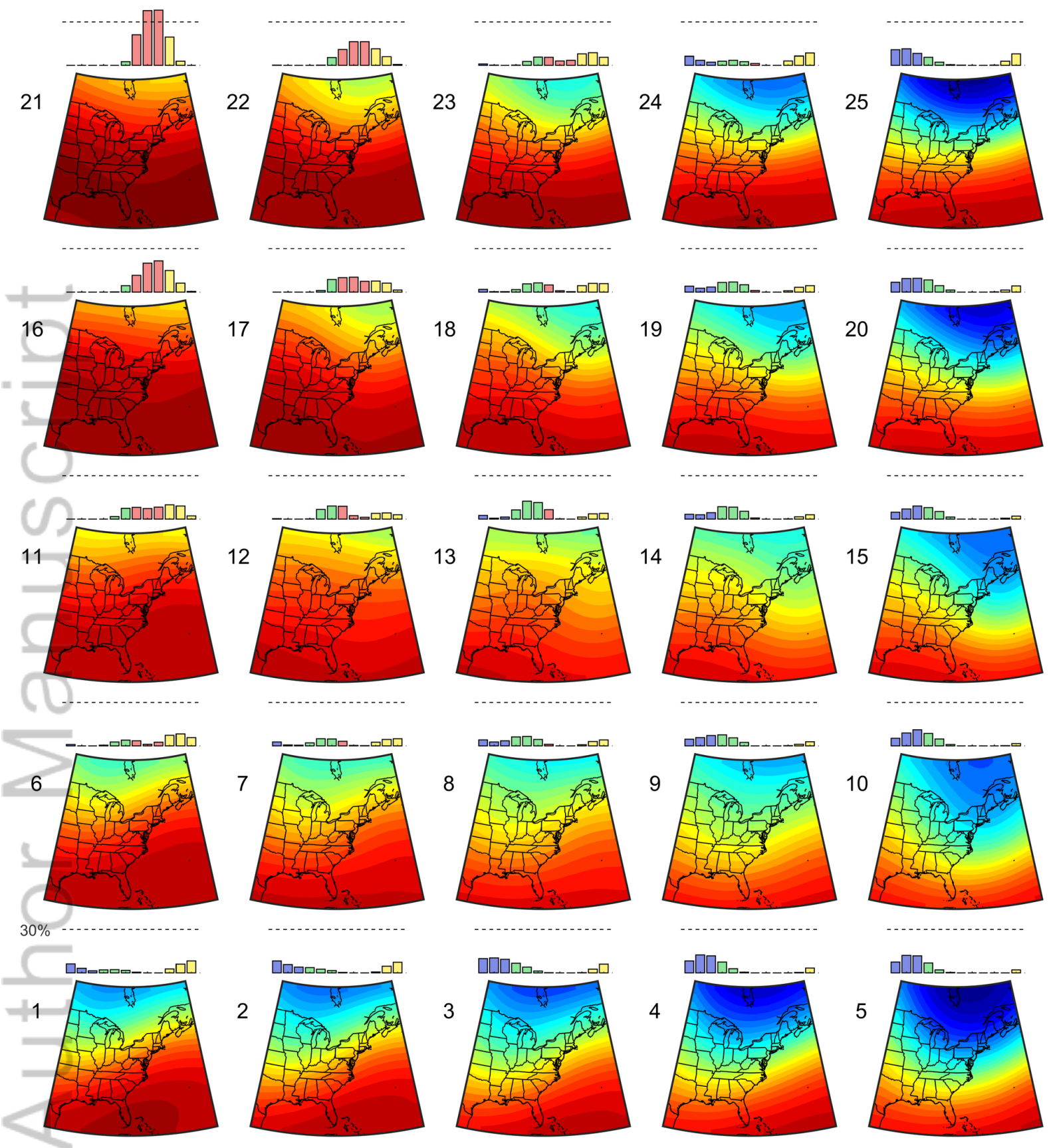

34	1	-1	4	4
-11	-4	2	-1	4
3	-2	-4	**-7**	-1
-3	-3	**-10**	-7	**-10**
7	3	-1	-1	-5

NARR

15	3	-1	2	5
-4	-2	1	-1	4
7	2	-3	-2	0
-2	-2	**-8**	-5	**-11**
4	2	-1	1	-3

ERA5

90	83	90	90	90
84	82	88	91	89
85	86	89	89	92
91	85	90	93	95
92	89	93	92	94

Match %

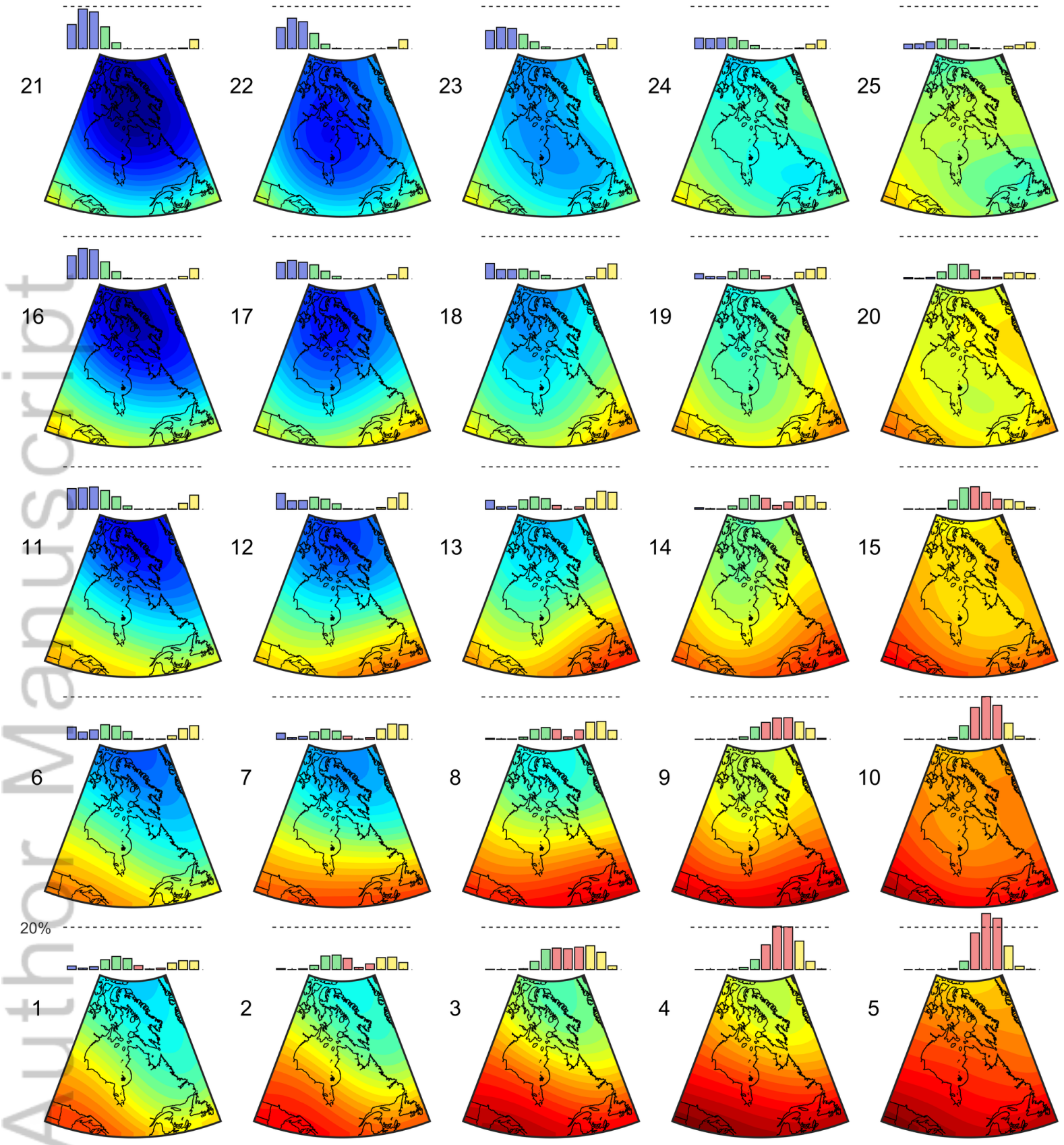

NARR				
-12	-1	6	1	1
-2	4	4	-1	-4
-7	-4	0	-2	-6
2	3	-3	0	***11***
-2	-4	0	-2	***23***

ERA5				
-9	0	6	0	1
-1	**5**	2	-1	-3
-5	-3	0	-2	-6
4	2	-3	1	***14***
-1	-5	-1	-6	***14***

Match %				
97	94	92	94	95
95	88	91	91	94
94	93	94	95	92
94	91	90	92	90
93	93	94	93	94

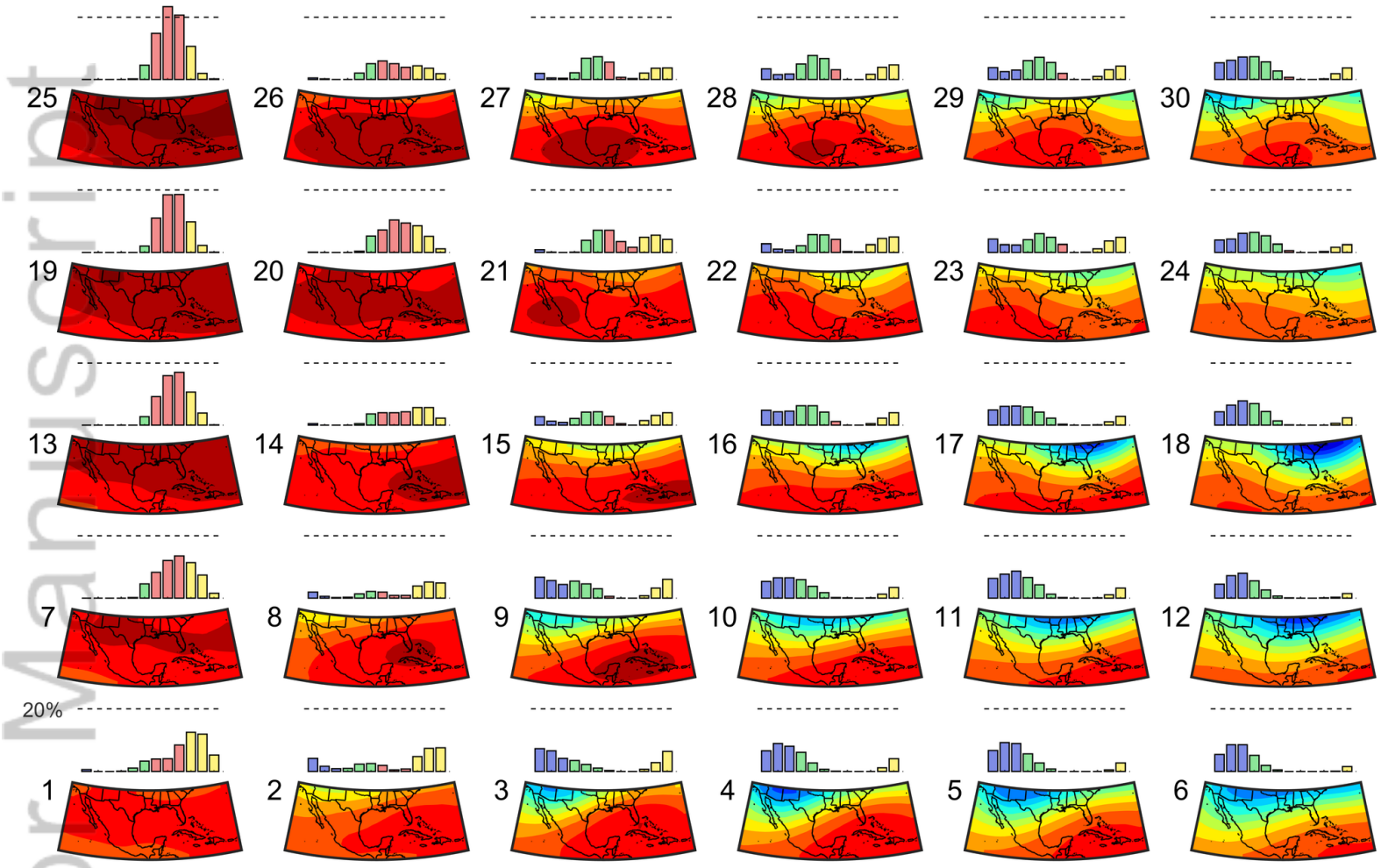

NARR					
37	**10**	**8**	**7**	-2	**-10**
4	**-11**	-3	-4	**-6**	**-7**
-1	**7**	**9**	5	2	**-9**
-12	2	**14**	**7**	-4	**-11**
-14	**-9**	4	0	**-6**	**-10**

ERA5					
21	5	4	**8**	1	**-8**
3	0	4	3	-1	-3
-6	**5**	**5**	5	**4**	**-7**
-5	1	**11**	4	-2	**-9**
-6	**-8**	-1	-2	**-6**	**-11**

Match %					
82	63	71	66	66	78
56	53	68	66	68	78
56	50	66	72	74	88
58	63	73	66	72	80
78	79	76	76	78	77

JOC_6983_Fig5.tif

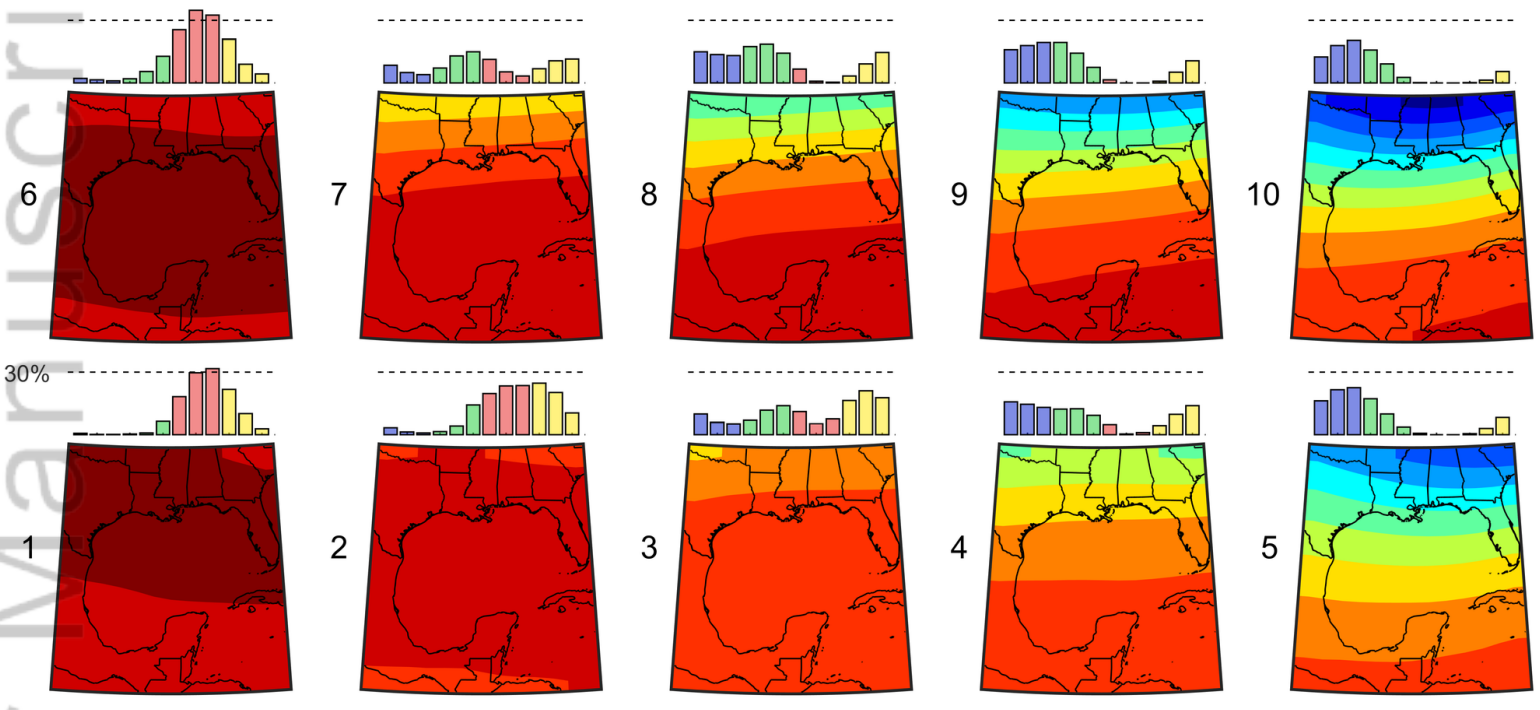

NARR				
85	***39***	***28***	***11***	***-13***
-16	***-36***	***-32***	***-37***	***-43***

ERA5				
21	***20***	***15***	-3	***-22***
13	-11	-5	***-13***	***-24***

Match %				
81	68	73	74	82
67	71	73	76	85

JOC_6983_Fig6.tif

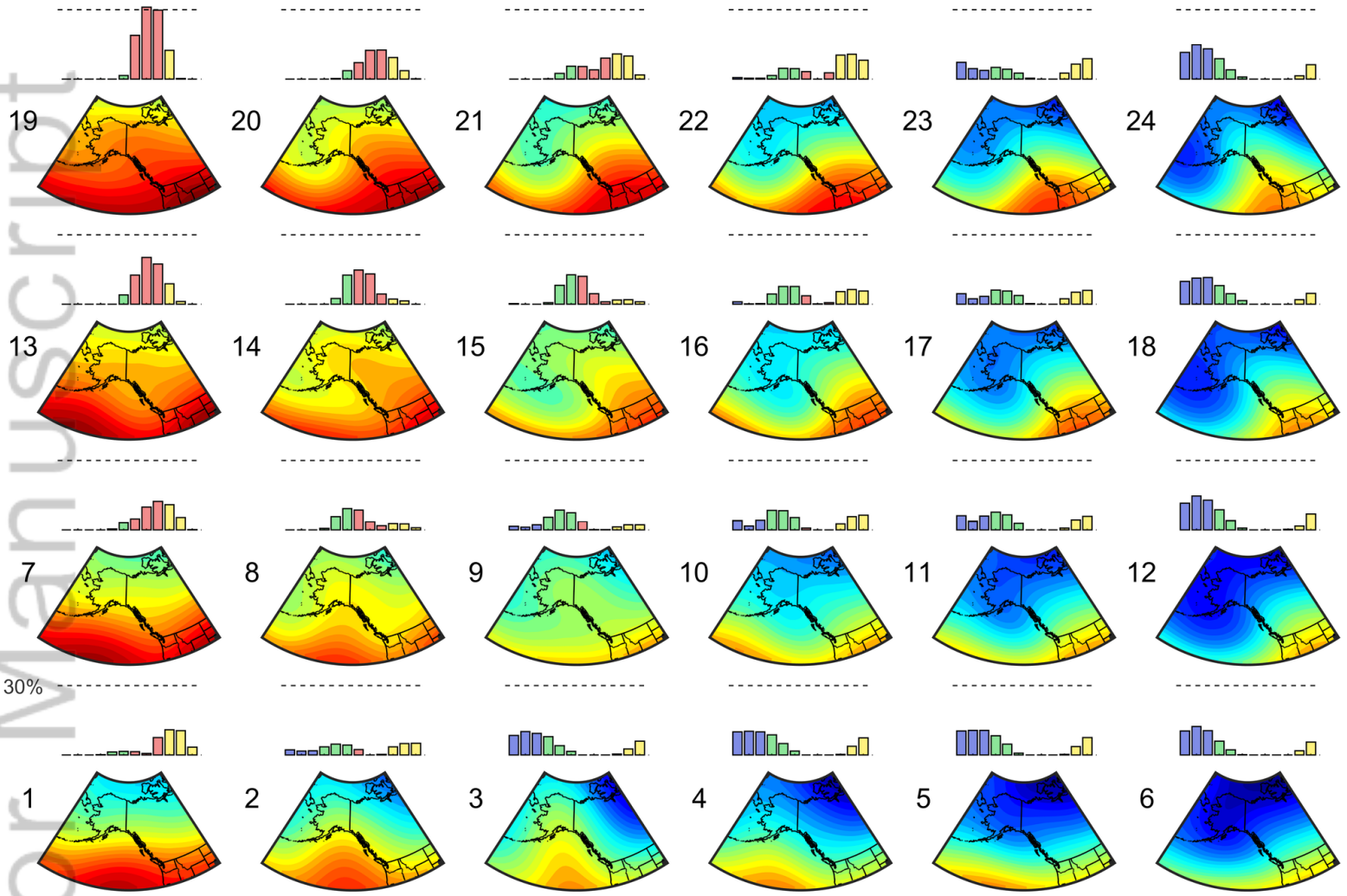

NARR					
18	1	-2	-2	**8**	-4
-3	1	-1	4	-3	-5
-1	2	-2	5	4	-6
0	-1	7	1	-2	-4

ERA5					
11	1	-2	-1	**8**	-3
-1	2	-1	4	-2	-5
0	3	-1	4	**5**	-5
0	-2	4	2	-3	-3

Match %					
97	93	96	93	92	95
93	93	92	92	90	94
94	93	93	91	92	95
95	96	95	95	92	95

JOC_6983_Fig7.tif

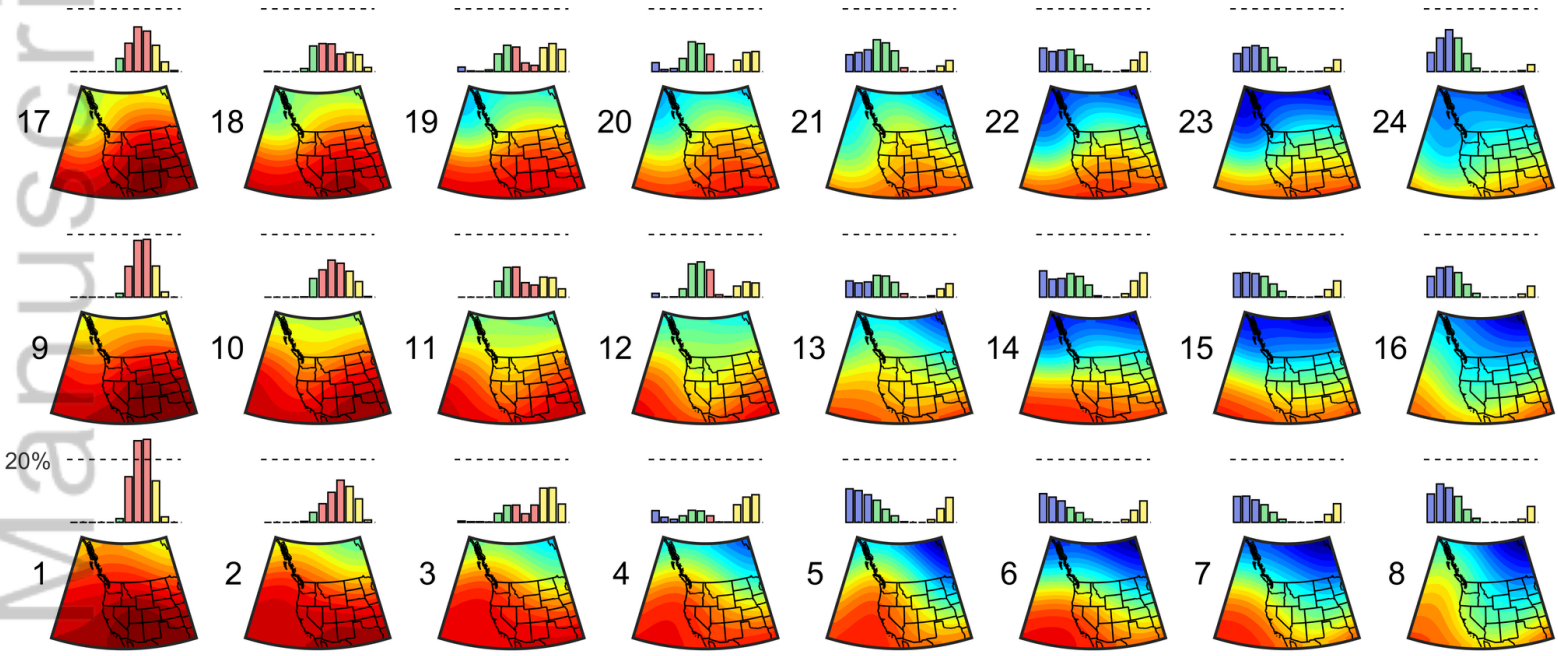

NARR							
-3	0	2	-3	-7	1	-1	-8
4	-2	**5**	0	-4	0	0	-3
18	-3	-6	2	6	**8**	1	**-9**

ERA5							
-5	-1	4	-4	-6	2	-2	-6
3	0	**5**	0	-2	2	0	-3
11	1	-4	3	4	**8**	1	**-9**

Match %							
91	91	91	90	92	90	92	95
89	90	91	90	88	91	92	93
96	90	93	93	94	90	88	95

JOC_6983_Fig8.tif

Assessing trends in atmospheric circulation patterns across North America

Erik T. Smith, Omon Obarein, Scott C. Sheridan, Cameron C. Lee

In this study, trends in atmospheric circulation patterns (CPs) from the North American Regional Reanalysis (NARR) and the recently released ERA5 datasets are compared. To create a more direct comparison between the CPs of each dataset, CPs from the ERA5 dataset are based on the principal components of the NARR dataset. 500mb geopotential height trends were generally larger than the mean sea-level pressure trends and the NARR CP trends tended to be larger than the ERA5 CP trends. Furthermore, the most extreme summer-dominant CPs were found to have increased significantly over the 40-year study period in all five regions for both the NARR and ERA5 CPs.

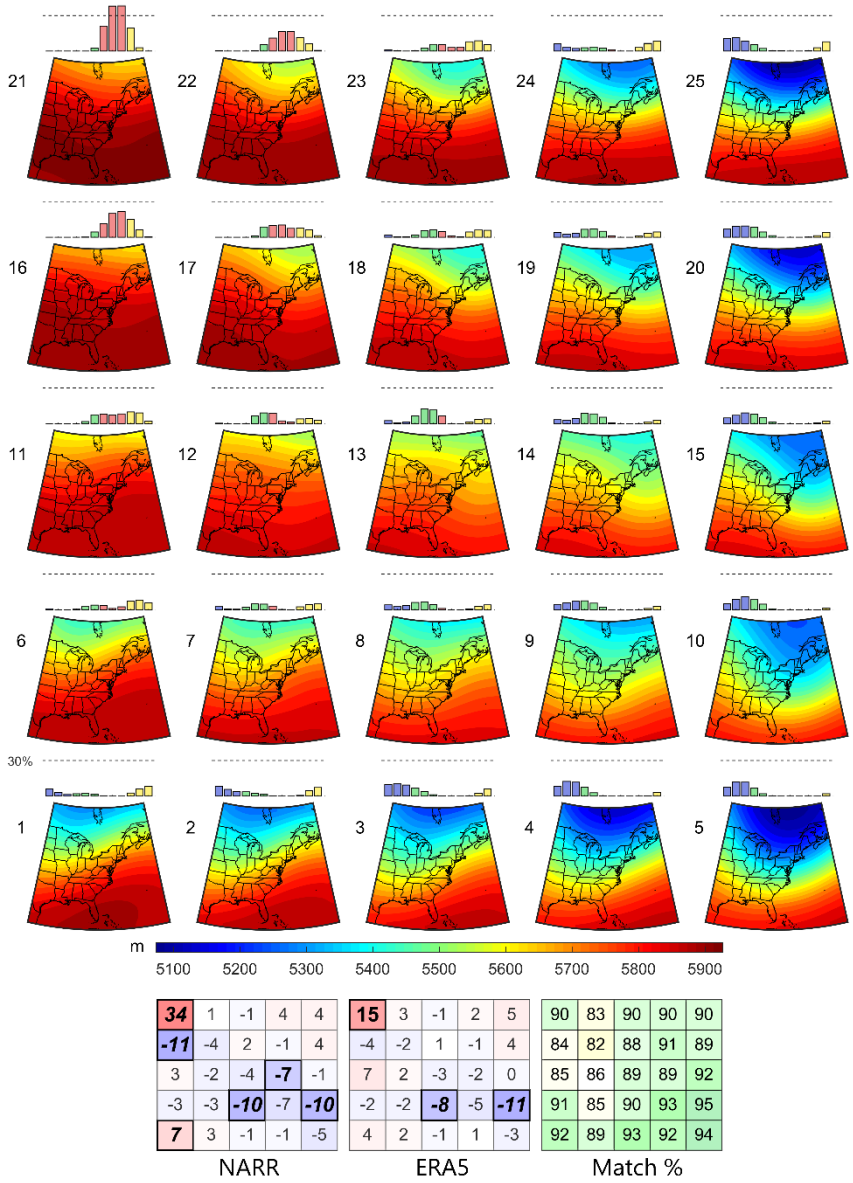

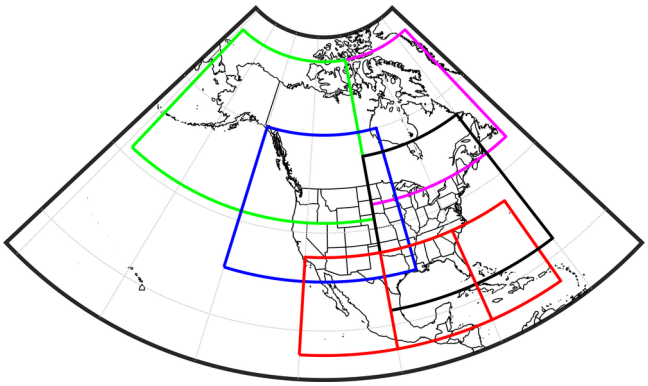

JOC_6983_Region_domians.tif

	NARR	ERA5
Domain	North America (15° N - 75° N and 52° W - 178° W)	NARR Domain
Period	1979 - 2018	1979 - 2018
Temporal Resolution	Daily mean	Daily mean
Spatial Resolution	~32 km upscaled to ~192 km	0.25° x 0.25° interpolated to match the upscaled NARR resolution (~192km)
Variables	MSLP and 500z	MSLP and 500z

JOC_6983_table1.PNG

	500z			MSLP		
Region	MAE (gpm)	Correlation	CP Match	MAE (hPa)	Correlation	CP Match
East	0.012	1.00	89%	0.025	0.99	85%
Gulf	0.030	0.98	69%	0.053	0.95	67%
West	0.010	1.00	86%	0.036	0.99	87%
North	0.011	1.00	88%	0.023	1.00	92%
Canada	0.008	1.00	87%	0.017	1.00	91%
New Gulf	0.018	0.96	78%	0.022	0.95	85%

JOC_6983_table2.PNG

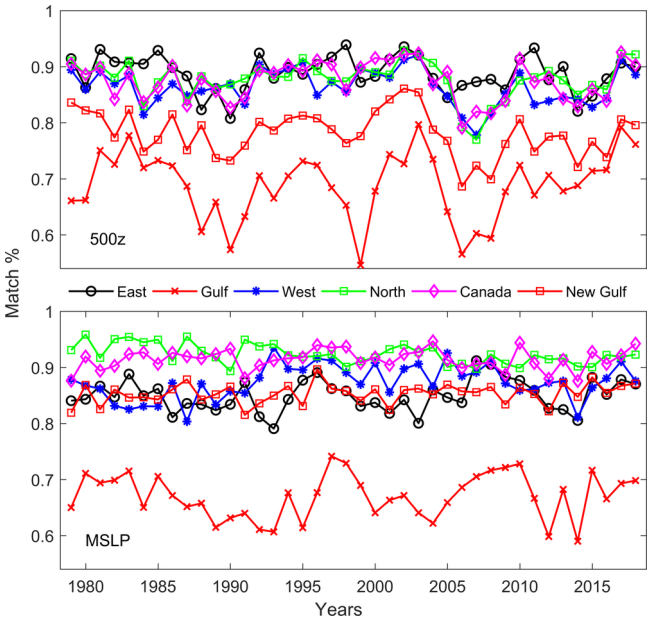

JOC_6983_year_match4.tif